Corrosion Science 82 (2014) 280–289

Contents lists available at ScienceDirect

Corrosion Science

journal homepage: www.elsevier.com/locate/corsci

Time-lapse synchrotron X-ray diffraction to monitor conservation coatings for heritage lead in atmospheres polluted with oak-emitted volatile organic compounds

Rosie Grayburn [a,c,*], Mark Dowsett [a], Michel De Keersmaecker [c], Eric Westenbrink [b], James A. Covington [b], James B. Crawford [a], Matthew Hand [a], David Walker [a], Pamela A. Thomas [a], Dipanjan Banerjee [d], Annemie Adriaens [c]

[a] Department of Physics, University of Warwick, Coventry CV4 7AL, UK
[b] School of Engineering, University of Warwick, Coventry CV4 7AL, UK
[c] Department of Analytical Chemistry, Ghent University, Krijgslaan 281 S12, B9000 Ghent, Belgium
[d] DUBBLE@ESRF (BM26), BP 220, 38043 Grenoble, France

ARTICLE INFO

Article history:
Received 27 November 2013
Accepted 23 January 2014
Available online 3 February 2014

Keywords:
A. Organic coatings
B. XRD
C. Atmospheric corrosion

ABSTRACT

We discuss the effectiveness of a lead tetradecanoate coating on lead to protect against harmful volatile organic compounds emitted from oak. The oak volatile organic compounds were characterized by GCMS and the major constituent was found to be acetic acid. Under the test conditions, the coating decreases the rate of corrosion by up to 75% compared to bare lead. The thickness of corrosion products on the sample was also calculated thus demonstrating the power of the time-lapse synchrotron radiation X-ray diffraction technique to deliver a quantitative estimate of the effectiveness of the coating.

1. Introduction

The release of volatile organic compounds (VOCs) from oak is a result of the biodegradation and metabolic processes within the wood [1,2]. The interaction between lead (and its alloys) and oak can be found in many cultural heritage contexts where the materials coexist in the same environment. For example, within a pipe organ, the lead-rich pipes can react with VOCs emitted by the oak wind chest [3–7] causing degradation of the pipe structure through pitting and cracking. As a consequence this can lead to a substantial loss of timbre within the instrument.

Other examples of VOC sources in cultural heritage contexts are found within museum display cases. Although many modern display cases attempt to explicitly omit wood and other VOC sources from their structure [8–11], antique wooden cases which have their own heritage value can still be found in use.

Long-chain carboxylic acids have been studied for possible use as protective coatings for heritage metals [12–16] as well as ancient building materials [17]. An aqueous solution of sodium carboxylates had been suggested by Rapin and co-workers [18] as a possible coating for heritage lead. Carboxylic acids $CH_3(CH_2)_{n-2}COOH$, where $12 \leqslant n \leqslant 18$, are virtually odorless but have limited or no solubility in water. In what follows we abbreviate these to C_n. Rocca and co-workers [19] deposited tetradecanoic acid (C_{14}) onto lead using the sodium salt of the carboxylate. The procedure for forming this coating was found to be complex due to the exact conditions required for layer formation [14,20].

We focus on exploiting the solubility of the carboxylates in ethanol as an alternative route for depositing long chain carboxylates onto lead. Not only does this simplify the deposition compared to the aqueous method but also it avoids possible corrosive effects from sodium salts used during the aqueous deposition method.

Tetradecanoic acid is highly soluble in ethanol (48.7 ± 0.5 g/100 mL) and, importantly for its potential as a conservation treatment, it is inexpensive and of low toxicity. It is widely used in pharmacology and the preparation of cosmetics.

The ethanolic solution is easy to produce and can be applied to metal surfaces by a variety of methods (dipping, painting, spraying). The carboxylic acid solution is applied to the lead surface and simply dried in air to form a uniform, near-invisible coating which we shall show is principally lead tetradecanoate ($Pb(C_{14}H_{27}O_2)_2$). The aim of this study is to measure the effectiveness of lead tetradecanoate as a protective coating against atmospheres polluted with oak-emitted volatile organic compounds in

* Corresponding author at: Department of Analytical Chemistry, Ghent University, Krijgslaan 281 S12, B9000 Ghent, Belgium.
E-mail address: rosie.grayburn@ugent.be (R. Grayburn).

http://dx.doi.org/10.1016/j.corsci.2014.01.027
0010-938X

enclosed and unventilated atmospheric environments. X-ray diffraction (XRD) measurements are used to identify corrosion products and observe the evolution of surfaces in real time and gas chromatography mass spectrometry (GC–MS) is used to identify the specific VOCs to which the samples were exposed.

2. Experimental

2.1. GC–MS of oak VOCs in the eCell

The eCell was set-up with an acrylic dummy sample holder in lieu of a lead sample and the oak environment created as described in the previous section with the humidity generator providing a relative humidity of 75%. The closed eCell environment was allowed to equilibrate for one hour prior to sampling. A custom-made septum plug attached a Restek IceBlue® Septa to the cell allowing collection of VOCs using a solid-phase microextraction (SPME) tip assembly (DVB/CAR/PDMS; 24 ga needle size; RS 57348-U, Restek, US). The tip was cleaned prior to exposure in the cell by running it three times through the GC–MS. It was then exposed to the environment within the cell for 5 min, 20 min or 3 h before being manually injected into the GC–MS (SCION-SQ™, Bruker). This involved exposing the fiber tip within the GC injector, which was kept at a constant temperature of 250 °C.

The resulting VOC gas sample was then split in the injector with a ratio of 1:10, allowing only one tenth of the sample through the column in order to sharpen the peaks on the eventual chromatogram. An initial column temperature of 50 °C was held for the first minute of the sample run, following which it was heated at a constant rate of 20 °C per minute to a maximum of 280 °C before being held constant for a further 2.5 min. This temperature profile was used to separate the different VOCs desorbed from the SPME fiber tip according to molecular weight, volatility and polarity before they were transmitted to the detectors.

2.2. Lead coupon preparation

Lead coupons with a diameter of 13 mm were pressed from 2 mm thick 99.95% lead metal sheet (Goodfellow Ltd., Cambridge, UK) and machined in an oil-free environment to a diameter of 12.5 mm.

One surface was then polished and cleaned using a protocol designed to eliminate as much preparation-related contamination as possible. This is as follows: The lead surface was polished by hand using a damp abrasive disc (BuehlerMet II ®) to remove visible surface defects and to expose a fresh metal surface. Coupons were then polished using a sequence of diamond polishes with decreasing particle sizes (6 μm, 3 μm, 1 μm Buehler MetaDi ® polycrystalline diamond suspension). A polishing cloth (Buehler MicroCloth ®) was saturated with the appropriate diamond suspension. A custom-made jig fitted to an automatic polisher (Buehler Minimet ® 1000) was used to hold the coupons in place during automated polishing. Coupons were polished for 15 min using each diamond suspension followed by rinsing with 2-propanol (99.5%, reagent grade) and cleaning in 2-propanol for 5 min in an ultrasonic bath. After polishing with the 1 μm diamond suspension, the coupons were ultrasonically cleaned in 2-propanol for 3 × 5 min, with fresh propanol for each cleaning cycle. Polished coupons were stored in 2-propanol until required.

2.3. Coating preparation

Tetradecanoic acid (1.14 g, 5 mmols, ⩾98% purum, Fluka Analytical) was dissolved in ethanol (100 mL, 99.99% reagent grade) to make a 0.05 M solution. Polished lead coupons were coated by immersing them in this solution overnight in a sealed beaker and then allowing them to dry naturally in air.

2.4. Ex situ experiments

To study some longer-term effects of oak VOCs on the coated lead, an oak polluted environment was created within a desiccator with a total volume of 800 cm^3. A total of 150 cm^3 of a saturated solution of sodium chloride at the base of the desiccator created an elevated relative humidity (RH): up to 75% for the ambient test temperatures (18–20 °C) [21]. Coated and uncoated lead samples were placed on a shelf alongside thirteen 1 cm^3 oak cubes within the desiccator for 2, 7 and 30 days. Coated and uncoated reference samples were simply left covered in air for the same period of time. The oak cubes were cut from a piece of contemporary oak (*Quercus* sp.) on a fine band saw to expose a fresh oak surface. The ratio of the oak surface area to air volume was 0.12 cm^{-1}.

Ex situ XRD measurements of samples exposed for 30 days to oak and laboratory air were taken on a PANalytical X'Pert Pro X-ray MRD X-ray powder diffractometer equipped with a curved Johansson monochromator giving pure Cu Kα X-rays at a wavelength of 1.540598 Å and a PIXcel detector allowing for faster data acquisition. The X-ray beam width was controlled using an automatic divergence slit to give a fixed 9 mm by 5 mm footprint on the sample. A 70 min $\theta - 2\theta$ scan from 1° to 70° 2θ with a step size of 0.0132° 2Θ was performed on each sample. Other *ex situ* measurements were performed using a Siemens D5000 diffractometer using Cu Kα X-rays with a wavelength of 1.5405 Å with a scintillation counter detector. A 185-min scan from 1° to 70° 2θ with a step size of 0.02° 2Θ was performed on each sample.

2.5. In situ experiments

Time-lapse *in situ* XRD measurements took place on a the DUBBLE beam line, ESRF within the eCell Mk IV, whose prototype is described elsewhere [22]. The eCell was created for *in situ* measurements on a synchrotron beam line and is designed to host a range of liquid or gaseous environments.

The largest possible oak annuli, which could fit into the eCell without obstructing the mechanism, were made. The objective was to achieve the highest partial pressure of VOCs in the shortest time with an oak surface area to cell volume ratio of 0.6 cm^{-1} so as to observe the effects on a time-scale compatible with a synchrotron experiment. The dimensions were: outside diameter 4.1 cm, inside diameter 2 cm, height 0.7 cm. After machining, the annuli were stored in a sealed container. A separate annulus was used for each experiment described below. A relative humidity of up to 75% was produced within the eCell by attaching a specially designed environment generator containing the saturated sodium chloride solution to one of the cell ports (see Fig. 1).

Two experiments are reported here: In the first, a coated lead coupon was exposed to oak VOCs from the annulus for 14 h with humidity controlled by the environment generator described above. In the second, a similar experiment was carried out on bare lead for 7 h. In this case oak VOC exposure was at the ambient RH of around 50%. Samples were placed on a sample holder within the cell, so that they could be automatically positioned around 200 μm from the X-ray window during XRD acquisition and then retracted to allow the environment unrestricted access to the surface.

Time-lapse interactions of lead samples with oak VOC atmospheres were studied using synchrotron X-ray diffraction (SR-XRD) at DUBBLE [23] (station BM26A, ESRF, Grenoble, France). X-rays with a wavelength of 1.5498 Å were incident at 10° to the surface producing a footprint of 1 mm × 200 μm. A Mar CCD 165 (Mar USA Inc., Evanston, IL, USA) 2D detector was used to record 2D diffraction patterns of the corroding lead surface. The axis of

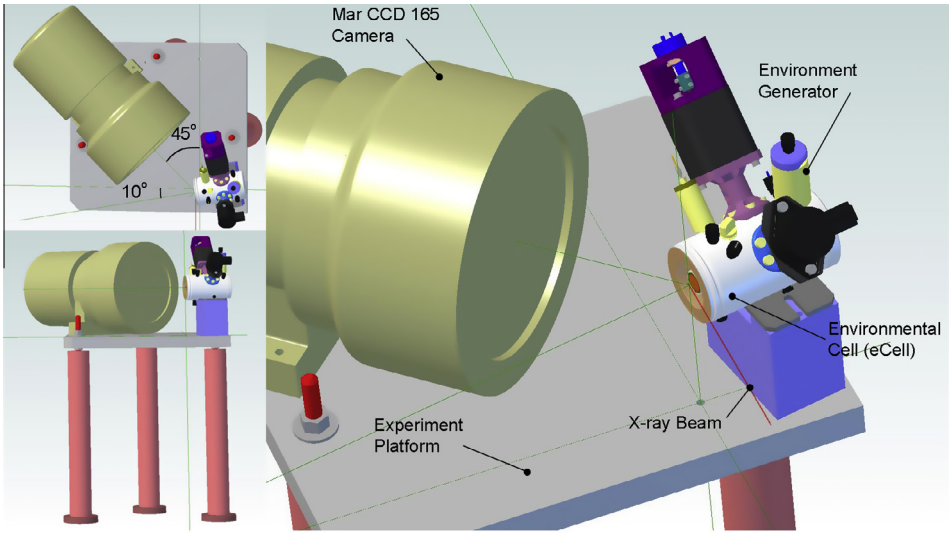

Fig. 1. The set-up on the DUBBLE beamline for time-lapse XRD of the effect of oak VOCs on the lead tetradeconate coating using the eCell MkIII and the Mar camera. The eCell is shown here with a Kapton window held in place by an O-ring. An oak annulus and an environment generator (cylinder, top) provide the corrosive environment.

the CCD camera was at 40.5° to the incident X-ray beam. The axial distance between the face of the detector and the beam center on the sample surface was 130 mm. Time-lapse sequences of images were collected, comprising XRD patterns with a 15-s exposure time recorded every 10 min for 14 h (coated lead) and 7 h (bare lead). A fast shutter was used to shield the sample from the X-rays between exposures.

All XRD data were processed using the group's esaProject 2013 software [24]. All extracted patterns were normalized to the beam monitor in order to account for beam decay. Patterns are given as intensity or counts vs. wave number Q ($=2\pi/d$ where d is the d-spacing), so that they can be compared on a common scale.

3. Results

3.1. GC–MS of Oak VOCs in the eCell

All peaks over 5×10^7 counts per second (cps) were identified (Table 1), using the NIST 2012 library. The compounds identified have been found in previous studies of oak emissions and museum environments [1,25–28] although the experimental methods are not directly comparable.

As VOC concentrations were allowed to accumulate in the oak VOC environment within the cell, the number of identifiable compounds increases according to the longer exposures of the SPME tip. However, the dominant component from all tip exposure-times is acetic acid. Fig. 2 shows that three times more acetic acid is emitted compared to any other compound. The high prevalence of acetic acid is probably due to its active production via a known degradation pathway [29,30]. Therefore lead is susceptible to interaction with acetic acid even during short periods of exposure to oak within the eCell.

Acetone, 2-butanone and acetic acid butyl ester also feature at all exposure times. Acetone was detected from reference solutions of acetic acid so it is presumed to originate from the ambient atmosphere, although it is also known to have biosynthetic origins [1].

Over twenty VOCs were identified from the GC trace after 3 h exposure to the oak environment, including an entire spectrum of saturated aldehydes from pentanal to dodecanal. The origin of these shorter-chain aldehydes in VOCs in unclear in literature but they could be degradation products as a result of prior heat-treatment of our wood sample [30]. Similarly furfural was only detected after 3 h tip exposure. This cyclic aldehyde is a product of cellulose dehydration, either from enzymatic action or as a result of prior heat-treatment of the wood sample [31]. Limonene,

Table 1
List of VOCs detected from oak within the eCell at 75% RH at various tip exposure times using GC–MS.

Time (minutes)	VOC (peak label)	SPME tip exposure time at which VOC is observed
1.320	Acetone (A)	5 min, 20 min, 3 h
1.914	2-Butanone (B)	5 min, 20 min, 3 h
2.270	Acetic acid (C)	5 min, 20 min, 3 h
2.645	2H-pyran-2-one (D)	3 h Only
2.858	Pentenal (E)	3 h Only
3.413	Toluene (F)	3 h Only
3.880	Acetic acid butyl ester (G)	5 min, 20 min, 3 h
4.420	Furfural (H)	20 min, 3 h
>4.420	Styrene (I), heptenal (J), benzaldehyde (K), octanal (L), limonene (M), nonanal (N), dodecanal (O), various other long-chain hydrocarbons	3 h only

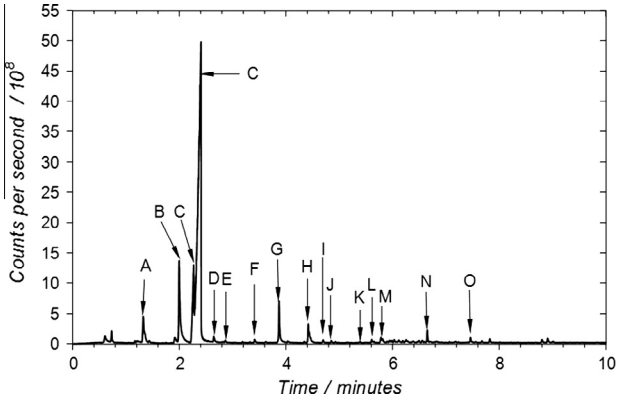

Fig. 2. GC trace after 3 h exposure of the SPME tip to the oak environment within the eCell. Peak labels are explained in Table 1. The peaks below 1 min are attributed to carbon dioxide.

a common terpene biosynthesised in plants [32], was detected after 3 h tip exposure. Limonene is not a degradation product of wood so low detection concentration suggests diffusion of limonene out of the wood rather than active production.

3.2. Corrosion of lead and coated lead by oak VOCs – long-term corrosion

Fig. 3a shows the XRD pattern of a tetradecanoate coated lead coupon measured on the PANalytical X-ray diffractometer. The fifteen peaks with a uniform spacing of 0.156 $Å^{-1}$ are the even reflections in the series 002, 004, ..., 0030, etc. which arise because the *c*-axis d-spacing is much larger than one wavelength. The odd reflections have a much lower intensity and the 001 peak is not visible, probably because of surface roughness. Although we can find no comparably high quality reference pattern for this compound, Fig. 3a shows a reasonable similarity to International Centre for Diffraction Database (ICDD) reference no. 00-049-1964 (lead tetradecanoate) and strong qualitative similarity to ICDD references for other long chain lead carboxylates such as lead hexadecanoate (No. 00-055-1624) and octadecanoate (No. 00-055-1625). It is quite distinct from the pattern measured from a thin layer of tetradecanoic acid on a Kapton® foil shown in the inset with the ICDD reference 00-008-0786. Work on fully indexing this pattern is incomplete, but the reflections labeled with asterisks between 1.4 and 1.8 $Å^{-1}$ are probably higher order reflections from the lead tetradecanoate lattice rather than from residual tetradecanoic acid.

Fig. 3b shows the XRD pattern of a tetradecanoate coated lead coupon after 30 days of storage in air measured on the PANalytical instrument. The data does not show any detectable crystalline corrosion products, thus demonstrating the effectiveness of the

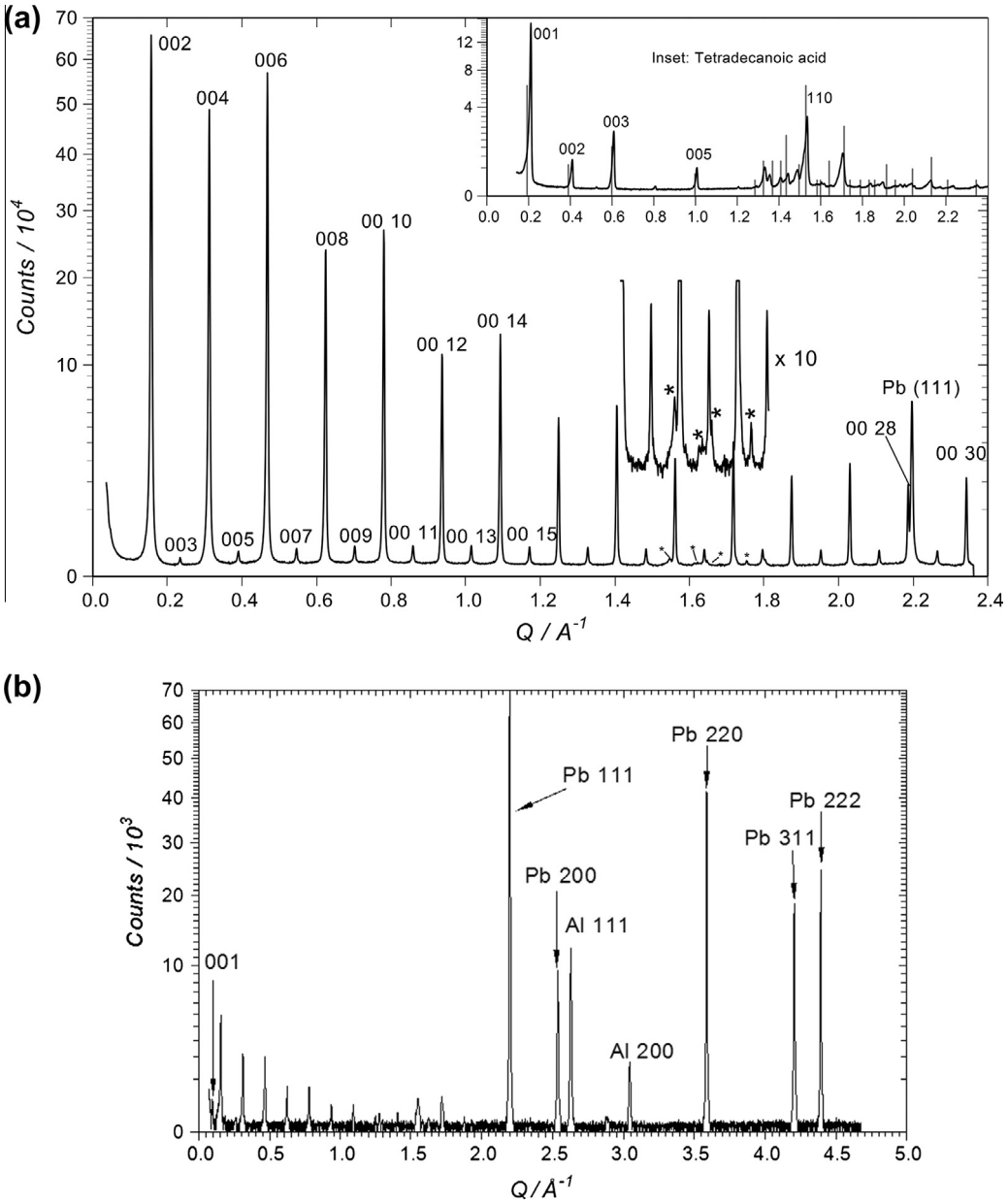

Fig. 3. (a) XRD pattern of the lead tetradecanoate coating taken a freshly prepared sample (5 h 20 min scan) with an inset showing the pattern from a thin layer of tetradecanoic acid on Kapton. The reflections labeled * in the main figure show possible locations of higher order lead tetradecanoate reflections. The 001 reflection from the coating is not visible but is present in the XRD pattern of tetradecanoic acid coated lead (b), stored in laboratory air for 30 days (3 h scan). The Al peaks are from the sample holder and shifted by the height difference between the lead and aluminum surfaces. The *y*-axis of the XRD patterns in this figure are shown on a square-root scale.

coating against appreciable corrosion in ambient conditions. The 001 reflection from the coating is visible in Fig. 3b. The other odd reflections are weak but just visible. The 00*n* reflection sequence in Fig. 3 is consistent with a *c*-axis spacing of 80.5 ± 0.1 Å. Lead reflections are also identified. The other peaks in Fig. 3b are due to the aluminum sample holder. The difference in relative intensity of the lead and lead tetradecanoate reflections between Fig. 3a and b suggests that the coating in the latter is thinner. Control of the coating thickness is still under investigation.

Fig. 4 shows raw (a) and reprojected [24] (b) Mar diffractograms from a lead tetradecanoate coated coupon acquired on DUBBLE. The acquisition time was 20 s. The bottom ring is at $Q = 0.7843$ Å^{-1} (peak 5 in Fig. 3). The coarse polycrystallinity of the lead coupon is demonstrated by the streaky nature of the lead rings. On the other hand, the evenly spaced rings which represent the lead tetradecanoate are smooth and homogenous which shows that the coating is formed from small polycrystals [14] randomly oriented in 2 directions, but with strong *c*-axis alignment indicated by the intensification in the in-plane scattering direction. The 1-D diffraction patterns from the Mar camera are simply integrated out of reprojected images, as shown in Fig. 4 (b), by summing image rows.

Fig. 5 summarizes the data from the exposure of lead to oak VOCs over periods of up to 30 days. In general, increased exposure times lead to increased backgrounds and loss of structure in the patterns. This can be attributed to four effects, viz: an increase in the number of peaks causing more overlap, broadening of peaks as long range order declines, the formation of amorphous phases, and deliquescence (frequently observed in environments with combined high RH and acetic acid concentrations [33].

Fig. 5a shows the progressive corrosion of the coated surfaces which were enclosed in the oak environment within a desiccator for 2, 7 (measured on the Siemens D5000 diffractometer) and 30 days respectively (measured on the PANalytical X-ray diffractometer). The most obvious effect of the oak environment after 2 days is the formation of lead acetate oxide hydrate (ICDD No. 18-1739) (see peak at 0.55 Å^{-1}). The GC–MS data show that acetic acid is the main VOC emitted from oak (Fig. 2), so it can presumed that this initial corrosion product derives from the reaction of acetic acid with the underlying lead, associated oxides and carbonates or with the coating itself.

Since these coatings are known to be hydrophobic we suppose that the reduction in pH of surface water through combination of water and acetic acid degrades this property. Then, the humid environment provides a thin film of water on the surface where acetate ions from dissolved gaseous acetic acid can form and react with lead. The association of these ions with the native oxide massicot, β-PbO (ICDD No. 38-1477) (peak at 2.0505 Å^{-1}) forms the lead acetate oxide hydrate compound. Massicot is formed during oak VOC exposure, but not on the protected surface left in air during the measurement period. After 7 days in an oak environment the peak area of the lead acetate oxide hydrate has halved, whilst the background due to amorphous and/or unresolved scattering has increased significantly. This is presumably due to ongoing corrosion and the breakdown of the lead acetate oxide hydrate to produce lead carbonates and re-form acetic acid – the oak VOC polluted environment (i.e. elevated humidity and acetic acid concentration) allows the breakdown of the acetate to the carbonate. Tétreault and co-workers found that plumbonacrite ($6PbCO_3 \cdot 3Pb(OH)_2 \cdot PbO$) was the favored corrosion product at 75% RH when lead was exposed to acetic acid, whereas hydrocerussite ($Pb_3(CO_3)_2(OH)_2$) was the preferred product at lower RH values and higher acetic acid concentrations [34]. In the oak polluted environment both hydrocerussite and plumbonacrite are formed because the elevated humidity causes a higher concentration of acetic acid to be released from oak [35,36]. This result is in agreement with Tétreault's findings.

All peaks of the lead tetradecanoate coating decrease in height with oak exposure (2 days compared to 7 days), which suggests either that the lead tetradecanoate layer is breaking down, or that it is being covered by the overgrowth of corrosion products, some of which may be amorphous [37]. Although a direct comparison between the 2 and 7 day data and the 30 day data cannot be made because the sensitivity and resolution of the PANalytical instrument are superior to the Siemens diffractometer, it can be seen that, even after 30 days, the 001 reflection and the even part of the 00*n* sequence are still visible (out to the 0010 reflection) and the sharp peaks are consistent either with coverage or the survival of a significant fraction of the coating intact.

Bare lead was also corroded within the same environment. A white layer of corrosion products formed within a few minutes exposure to the oak VOCs. Fig. 5b shows the XRD results of bare lead kept with oak for 2 and 7 days measured on the Siemens D5000 diffractometer. The higher background for the 7-day exposure could be due to the formation of a large number of different corrosion products leading to the coalescence of unresolved small peaks, the growth of amorphous corrosion products, or even some deliquescence. Strong diminution in the lead reflections (e.g. 111 and 311) due to the coverage of corrosion products is evident. The small lead acetate peak demonstrates advanced corrosion compared to the coated lead, and lead carbonate has formed already after 2 days. Lead acetate is an important intermediate to lead carbonate formation [33] therefore corrosion occurs more rapidly when lead is uncoated.

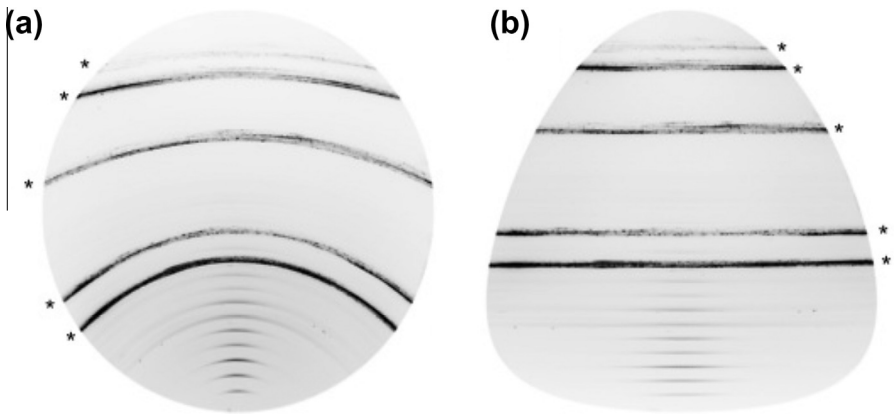

Fig. 4. Raw (a) and reprojected [24] (b) Mar SR-XRD diffractograms from a lead tetradecanoate coated coupon acquired on DUBBLE beamline, ESRF. The acquisition time was 15 s. Lead reflections are denoted by a *.

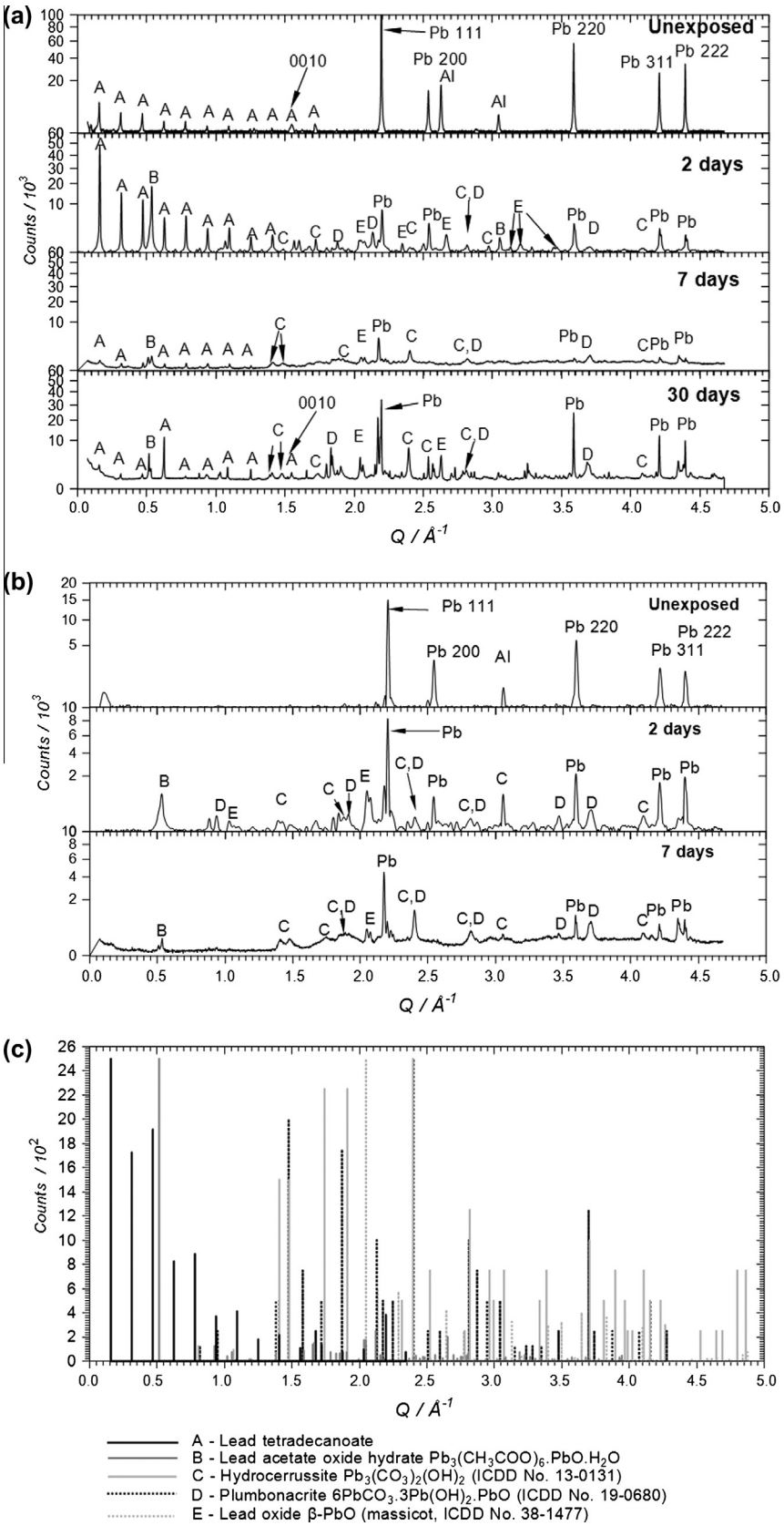

Fig. 5. (a) XRD patterns of lead tetradecanoate coated lead coupons after 2, 7 and 30 days within an oak environment. These patterns are compared to the XRD pattern from an unexposed coated coupon. Aluminum peaks derive from the sample stage. (b) XRD patterns of bare lead coupons after 2 and 7 days within an oak environment compared with an unexposed lead coupon. The *y*-axis of the XRD patterns in a and b are shown on a square-root scale. Diffraction patterns are compared against reference diffraction patterns in (c). The reference diffraction pattern for lead is shown in Fig. 8.

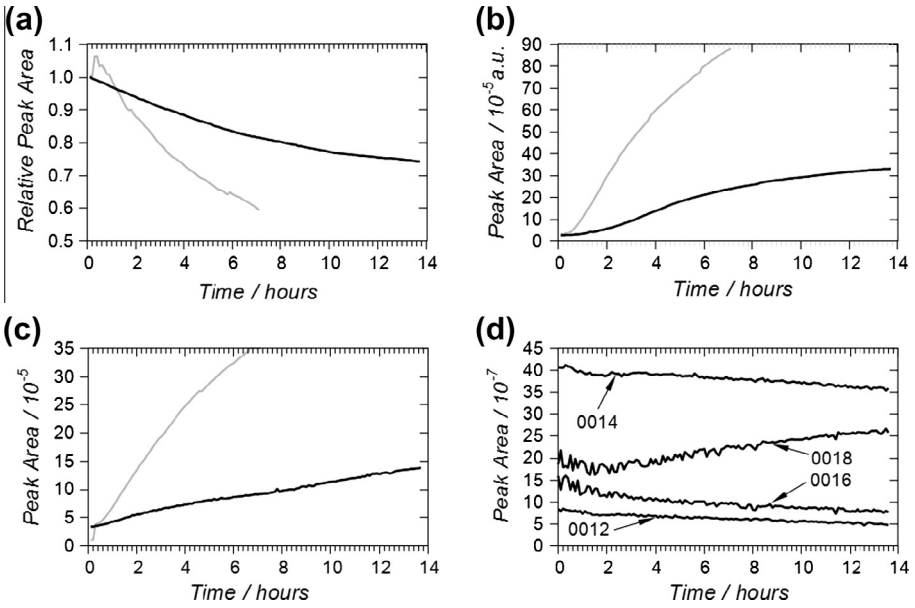

Fig. 6. Corrosion of the lead tetradecanoate coating in real time (elevated humidity, oak environment) and comparison with bare lead corrosion (ambient humidity, oak environment). Peak areas were extracted from (a) lead (1 1 1) @ 2.21 Å^{-1}, (b) massicot (β-PbO) (0 1 0) @ 2.07 Å^{-1}, (c) hydrocerussite ($Pb_3(CO_3)_2(OH)_2$) (0 0 3) @ 1.91 Å^{-1}, and (d) lead tetradecanoate even reflections from (0 0 1 2) to (0 0 1 8).

3.3. Corrosion of lead and coated lead by oak VOCs – SR-XRD time-lapse corrosion study

Fig. 6 shows the background corrected peak areas of lead, massicot (β-PbO), hydrocerussite ($Pb_3(CO_3)_2(OH)_2$) and the lead tetradecanoate coating extracted from the sequences of SR-XRD diffractograms recorded from the eCell containing the oak annulus to generate VOCs. The coated lead was exposed over a period of 14 h (85 images) with RH rising to 75%. The bare lead was exposed for 7 h (43 images) at ambient RH ~50%. The difference in relative humidity between experiments is important because increased relative humidity not only accelerates acetic acid emission from oak [35,36] but also enhances corrosion directly due to the presence of a thicker electrolyte layer. Data from coated lead are delineated in black, whilst those from bare lead are in grey.

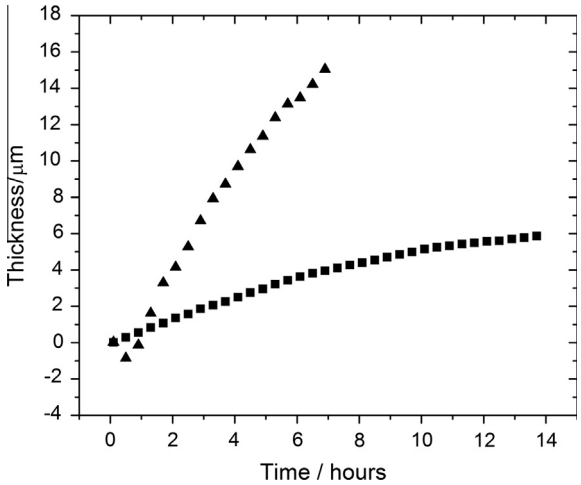

Fig. 7. Thickness of hydrocerussite growing on coated (squares) and uncoated (triangles) lead with time. Mass thickness is calculated by translating Fig. 6a data into the Eq. (3). Thickness of the coating uses the mass thickness divided by the density of hydrocerussite.

Fig. 6a shows the time dependence of the area of the lead 1 1 1 peak at 2.21 Å^{-1}. For each set, the areas have been normalized to that of the first peak in the set. Peak area data for the remaining lead reflections when manipulated in the same way give very similar results. The peak from the bare lead actually increases by 5% during the first 4 patterns. This is an artifact of the measurement process: the polycrystalline lead surface re-orientates somewhat with the onset of corrosion. The observed overall decrease in the peak areas is due to increasing coverage by corrosion products, which absorb both the incoming beam and X-rays scattered from the lead surface. For both coated and bare lead the behavior is characteristic of corrosion growth, which passivates somewhat, but there is appreciably less corrosion on the coated lead at any given time. Below, we use these data to obtain a semi-quantitative estimate of the corrosion layer thickness.

Peak areas from a surface layer which grows without structural change or being itself covered will increase to an asymptotic value because, once the corrosion layer is sufficiently thick to absorb or scatter all the incoming beam, no further increase in peak area (or height) will occur. This behavior is convolved with any tendency for growth to passivate, and cannot be modeled unless the growth law is known or assumed. Nevertheless, direct comparisons between the data from coated and bare lead can be made as follows.

Fig. 6b shows the change in lead (II) oxide (β-PbO, massicot) 0 1 0 peak at 2.07 Å^{-1} area over time. The amount of detectable lead oxide at any time after the first 30 min is around four times greater for the uncoated sample. Some oxide is present on both samples from the start – the polished lead surface has already been exposed to air for a few minutes. Rapid growth does not start for 20–30 min, possibly reflecting the time taken for the atmosphere (RH, oak VOCs) in the cell to stabilize. Although native oxide growth results from direct contact of lead with oxygen in the air (Reaction (1)), its production can be increased as a result of acetic acid exposure [38]. This is due to the formation of lead acetate oxide hydrate, which uses the native PbO in its formation (Reactions (2) and (3)): the

dissolved acetate ions promote the reaction of the underlying lead with air to produce β-PbO.

$$2Pb + O_2 \rightarrow 2PbO \quad \text{(Reaction1)}$$

$$PbO + 2CH_3COOH \rightarrow Pb(CH_3COO)_2 + H_2O \quad \text{(Reaction2)}$$

$$3Pb(CH_3COO)_2 + PbO + H_2O \rightarrow Pb_3(CH_3COO)_6 \cdot PbO \cdot H_2O \quad \text{(Reaction3)}$$

The concentration of acetic acid forming on the surface is not likely to be the same in the coated lead and uncoated lead and the position of the water film is different. At the least, the long carbon chains of the lead tetradecanoate coating form a hydrophobic barrier on the surface of the lead which reduces the amount of water into which acetic acid vapor can dissolve whilst placing a barrier between this and the surface. It therefore takes longer for the corrosive agents to reach the lead surface promote the formation of β-PbO and the down-stream reaction products.

Fig. 6c shows the changes in peak area with time for the hydrocerussite 003 peak at 1.9 $Å^{-1}$. The peak areas of this corrosion product on coated lead are six times lower than for the bare lead 6 h into exposure. These results demonstrate the protection afforded by the coating. Hydrocerussite growth results from the reaction of lead with acetic acid emitted from the oak. As discussed previously, lead acetate oxide hydrate breaks down to form carbonates and simultaneously reform acetic acid (Reaction 4).

$$3Pb_3(CH_3COO)_6 \cdot PbO \cdot H_2O + 8CO_2 + 10H_2O \rightarrow 4Pb_3(CO_3)_2(OH)_2 + 18CH_3COOH \quad \text{(Reaction4)}$$

Lead acetate oxide hydrate cannot be seen on the diffraction patterns due to the low angle limitation of the instrumental setup – the lead acetate peak would be expected at 0.5 $Å^{-1}$ but the measurement limit with our Mar configuration is 0.6 $Å^{-1}$ (to prevent secondary scattering off the camera bezel). Despite the lack of an acetate peak it can be deduced from the longer-term oak exposure data (Fig. 5) that lead acetate is the cause of hydrocerussite formation.

Fig. 6d shows the change in peak areas of the even lead tetradecanoate peaks from 0012 to 0018 over time within the oak environment. At longer oak exposure times (see Fig. 5) it was found that the coating peaks apparently diminish over days, but this could be due to the eventual build up of corrosion products on the surface – results from reflections 0012 to 0016 show the initial signs of this long-term behavior. The peak areas of the lead tetradecanoate coating in Fig. 6d suggests the location of corrosion is initially between the coating and the lead surface since the corrosion product growth seen in Fig. 6a–c do not proportionally diminish the tetradecanoate reflections. The peak areas for the 0014 reflection are more than double that of the 0012 and 0016 reflections but the peak areas of the even reflections from 0012 to 0016 reduce by 6.25%, 11.25% and 46.7% respectively during the 14-h measurement period. This implies that the higher order the reflection, the more sensitive the reflection is to surface coverage by corrosion products. The 0018 reflection increases by 30% during the measurement period due to proximity to the growing plumboacrite peak, which overlaps into the integration limit for this carboxylate reflection.

In order to obtain more quantitative information on the protection afforded by the coating, we proceed as follows: We assume that the X-ray absorption follows the Beer–Lambert law. Then, provided the lead peaks only cover a small range of angle so that the input and exit paths can be considered invariant over the peak we can write

$$A(t) = R(t)A_0 \exp\left(-\frac{\mu}{\rho}d(t)k\right) \quad (1)$$

where $A(t)$ is the time dependence of the area of the lead 111 reflection, $R(t)$ corrects for changes in the reflection coefficient from the lead surface (e.g. due to changes in orientation as described above), A_0 is the peak area for no attenuation and for $R = 1$, μ/ρ is a mean mass absorption coefficient for the corrosion layer, ρ is its mean density, $d(t)$ is the mean mass thickness (mass per unit area) of the corrosion, and k is a constant which accounts for the experimental geometry:

$$k = \frac{1}{\sin\theta_i} + \frac{1}{\sin(2\theta - \theta_i)} \quad (2)$$

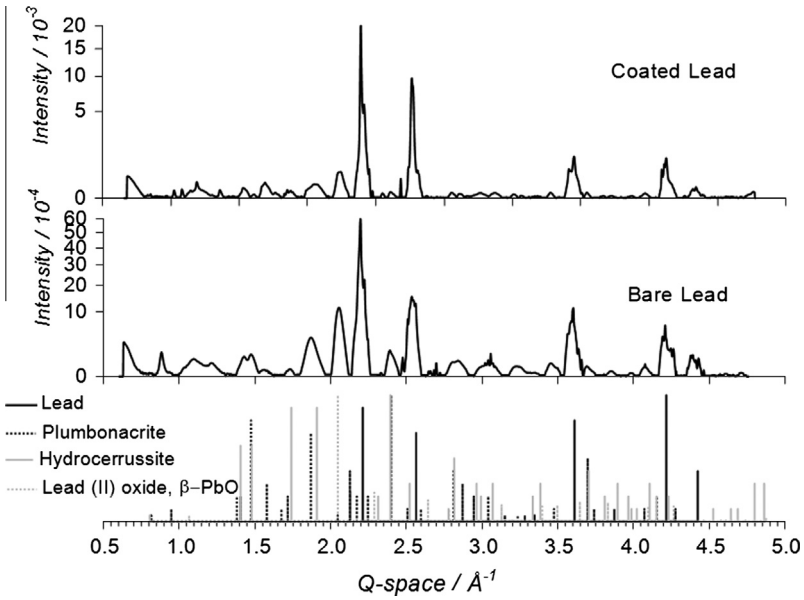

Fig. 8. Final SR-XRD patterns of lead and tetradecanoate coated lead after exposure to oak VOCs within the eCell, i.e. the spectra used to calculate the last data point in Fig. 6. Diffraction patterns are compared against reference diffraction patterns for hydrocerussite (ICDD No. 13-0131), plumbonacrite (ICDD No. 19-0680), massicot (ICDD No. 38-1477) and lead. The *y*-axis of the XRD patterns in this figure are shown on a square-root scale.

where θ_i is the incident angle of the beam to the surface (10°), and 2θ is the scattering angle for the 1 1 1 reflection. Clearly, this expression includes the simplifying assumption that μ/ρ remains constant over time.

The growth law for the corrosion $d(t)$ can be obtained directly by transforming the data in Fig. 6a according to

$$d(t) = \frac{\rho}{\mu k} \ln\left(\frac{R(t)A_0}{A(t)}\right) \quad (3)$$

In general, the use of a 2-D detector followed by integration along the rings will make the data less sensitive to changes in R compared to a scanned point or linear detector, and, although the first 4 data points for the bare lead show an abrupt 5% increase which we attribute to a change in R this is relatively small. Therefore, for the purposes of obtaining an estimate of $d(t)$ we set R to 1.

By applying Eq. (3) to the data in Fig. 6a, using the mass absorption coefficient for hydrocerussite calculated using NIST data [39] we can calculate the mass thickness of hydrocerussite on coated and uncoated lead. The values of mass absorption coefficients are similar for massicot (198 cm^2/g), plumbonacrite (191 cm^2/g) and hydrocerussite (179 cm^2/g) therefore the mass thicknesses calculated for all corrosion products are comparable. This quantification exercise also gives us information on the thickness of this corrosion product on the sample surface by simply dividing the mass thickness results by the density of hydrocerussite, 6.8 g/cm^3.

The behavior of hydrocerussite thickness over time is shown in Fig. 7. As explained previously for Fig. 6a, the initial decrease in thickness of the corrosion layer on lead is an artifact of the measurement process. After 4 h, the thickness of hydrocerussite on coated lead is 2.0 μm whereas it grows to a thickness of 10 μm on bare lead after the same period of time. So, the coating is significantly retarding the growth of corrosion products on the lead surface. As with the data in Fig. 6a, the thickness of hydrocerussite is tending towards asymptotic behavior due to passivation of the surface and absorption by the corrosion layer of incoming X-rays. However, the protective coating will reduce the hydrocerussite thickness on coated compared to bare lead by up to 75%.

Fig. 8 shows the final diffraction patterns of bare and coated lead after exposure to oak within the eCell. As expected from Fig. 6, the peak areas of lead oxide and lead carbonate corrosion products are greater for the bare lead, again demonstrating the protective nature of the coating. The peaks are broader than from a laboratory diffractometer because of the inherently low the angular resolution inherent in our experimental geometry on the synchrotron.

4. Conclusion

A study of the effectiveness of a lead tetradecanoate coating on lead to protect against harmful VOCs emitted from oak was conducted using time-lapse SR-XRD *in situ* and laboratory XRD. SPME GC–MS was used to characterize the VOCs themselves.

Acetic acid was confirmed as the most predominant VOC emitted from oak (*Quercus* sp.), being three times more prevalent than any other. Acetic acid was also the only reactive VOC, detected, reacting with lead to produce lead acetate oxide hydrate as a precursor to other corrosion products such as hydrocessurite. There was no evidence to show that other VOCs such as long-chain aldehydes reacted with the bare lead. The laboratory experiments showed that the coating was still present after 30 days, but became visibly patchy, or covered with corrosion products.

By studying the growth of corrosion products it was found that the coating reduces the growth rates of some corrosion products by up to 75% compared with bare lead, and generally inhibits attack from the VOCs. However corrosion products still form, initially at the metal-coating interface. From the time-lapse XRD data it was also possible to estimate the thickness of hydrocerussite growing as a function of time on the bare and coated coupons.

Acknowledgment

The authors would like to thank Franc Sever (ESRF Software Support), The Eveeson Charitable Trust and BROAD US Foundation for funding the GCMS equipment, Derrick Richards and Adrian Lovejoy for the construction of the eCell and related electronics, and Sandra Greck (IPSO FACTO, Marseilles) for identification of the oak. The PANalytical MRD diffractometer used in this research was obtained through the Science City Energy Futures Project: Hydrogen Energy, with support from Advantage West Midlands (AWM). esaProject and the eCell design are copyright 2013 Dowsett and Adriaens, and made available by EVA Surface Analysis. Also support from the Fund for Scientific Research – Flanders (FWO) is gratefully acknowledged.

References

[1] J. Kesselmeier, M. Staudt, Biogenic volatile organic compounds (VOC): an overview on emission, physiology and ecology, J. Atmos. Chem. 33 (1999) 23–88.
[2] E. Roffael, Volatile organic compounds and formaldehyde in nature, wood and wood based panels, Holz Als Roh-Und Werkstoff 64 (2006) 144–149.
[3] C. Chiavari, C. Martini, D. Prandstraller, A. Niklasson, L.-G. Johansson, J.-E. Svensson, A. Åslund, C.J. Bergsten, Atmospheric corrosion of historical organ pipes: the influence of environment and materials, Corros. Sci. 50 (2008) 2444–2455.
[4] A. Niklasson, L.-G. Johansson, J.-E. Svensson, Influence of acetic acid vapor on the atmospheric corrosion of lead, J. Electrochem. Soc. 152 (2005) B519.
[5] A. Niklasson, S. Langer, K. Arrhenius, Air pollutant concentrations and atmospheric corrosion of organ pipes in European church environments, Stud. Conserv. 53 (2008) 24–40.
[6] F. Deflorian, M. Fedel, Electrochemical analysis of the degradation of lead alloy organ-pipes due to acetic acid, J. Cultural Heritage. (2012).
[7] A. Åslund, J. Speedstra, The COLLAPSE Project: Corrosion of Organ Pipes – Causes and Recommendations, Publications Office of the European Union, Luxembourg, 2011.
[8] C. Degrigny, R. Le Gall, Conservation of ancient lead artifacts corroded in organic acid environments: electrolytic stabilization/consolidation, Stud. Conserv. 44 (1999) 157–169.
[9] D. Martin, High-performance display cases, Museum Practice 2 (1999) 42–45.
[10] N.H. Tennent, J. Tate, L. Cannon, The corrosion of lead artifacts in wooden storage cabinets, S.S.C.R. Journal 4 (1993) 8–11.
[11] D. Wegner, Lead corrosion in exhibition ship models, Nautical Res. J. 43 (1996) 32–40.
[12] K. De Wael, M. Keersmaecker, M. Dowsett, D. Walker, P.A. Thomas, A. Adriaens, Electrochemical deposition of dodecanoate on lead in view of an environmentally safe corrosion inhibition, J. Solid State Electrochem. 14 (2009) 407–413.
[13] M. Dowsett, A. Adriaens, B. Schotte, G. Jones, Real time spectroelectrochemical growth and corrosion resistance monitoring of lead carboxylate coatings in an environmental cell (eCell), in: C. Degrigny, R. van Langth, I. Joosten, B. Ankersmit (Eds.), Proceedings of the Interim Meeting of the ICOM-CC Metal Working Group, Amsterdam, 17–21 September 2007, n.d. pp. 26–31.
[14] M. Dowsett, A. Adriaens, B. Schotte, G. Jones, L. Bouchenoire, In-situ spectroelectrochemical study of the growth process of a lead decanoate coating as corrosion inhibitor for lead surfaces, Surf. Interface Anal. 41 (2009) 565–572.
[15] A. Adriaens, M. Dowsett, Time resolved spectroelectrochemistry studies for protection of heritage metals, Surf. Eng. 24 (2008) 84–89.
[16] A. Adriaens, F. De Bisschop, M. Dowsett, B. Schotte, Growth and real time corrosion resistance monitoring of lead decanoate coatings, Appl. Surf. Sci. 254 (2008) 7351–7355.
[17] R.A. Walker, K. Wilson, A.F. Lee, J. Woodford, V.H. Grassian, J. Baltrusaitis, G. Rubasinghege, G. Cibin, A. Dent, Preservation of York Minster historic limestone by hydrophobic surface coatings, Sci. Rep. 2 (2012) 880.
[18] C. Rapin, A. D'Huysser, J.-R. Labbe, L. Gengembre, P. Steinmetz, Etude de l'inhibition de la corrosion aqueuse du cuivre par les carboxylates linéaires saturés. II. Caractérisation des films superficiels formés par réaction entre le cuivre et l'anion heptanoate, Revue de Metallurgie. Cahiers D'Informations Techniques 93 (1996) 719–727.
[19] E. Rocca, J. Steinmetz, Inhibition of lead corrosion with saturated linear aliphatic chain monocarboxylates of sodium, Corros. Sci. 43 (2001) 891–902.
[20] B. Schotte, A study of the electrolytic reduction of corroded lead objects and the application, characterization and testing of a protective lead carboxylate coating, PhD Thesis, Universiteit Gent, Belgium, 2007.
[21] L. Greenspan, Humidity fixed points of binary saturated aqueous solutions, J. Res. National Bureau Standards. Sect. A: Phys. Chem. 81 (1977) 89–96.

[22] M.G. Dowsett, A. Adriaens, Cell for simultaneous synchrotron radiation X-ray and electrochemical corrosion measurements on cultural heritage metals and other materials, Anal. Chem. 78 (2006) 3360–3365.
[23] S. Nikitenko, A.M. Beale, A.M.J. van der Eerden, S.D.M. Jacques, O. Leynaud, M.G. O'Brien, D. Detollenaere, R. Kaptein, B.M. Weckhuysen, W. Bras, Implementation of a combined SAXS/WAXS/QEXAFS set-up for time-resolved in situexperiments, J. Synchrotron Radiat. 15 (2008) 632–640.
[24] A. Adriaens, M. Dowsett, K. Leyssens, B. Van Gasse, Insights into electrolytic stabilization with weak polarization as treatment for archaeological copper objects, Anal. Bioanal. Chem. 387 (2007) 861–868.
[25] G. Konig, Relative contribution of oxygenated hydrocarbons to the total biogenic VOC emissions of selected mid-European agricultural and natural plant species, Atmos. Environ. 29 (1995) 861–874.
[26] A. Fenech, M. Strlič, I. Kralj Cigić, A. Levart, L.T. Gibson, G. de Bruin, K. Ntanos, J. Kolar, M. Cassar, Volatile aldehydes in libraries and archives, Atmos. Environ. 44 (2010) 2067–2073.
[27] M.S. Pérez-Coello, J. Sanz, M.D. Cabezudo, Gas chromatographic-mass spectrometric analysis of volatile compounds in oak wood used for ageing of wines and spirits, Chromatographia 47 (1998) 427–432.
[28] M. Risholm-Sundman, M. Lundgren, E. Vestin, P. Herder, Emissions of acetic acid and other volatile organic compounds from different species of solid wood, Holz Als Roh-Und Werkstoff 56 (1998) 125–129.
[29] D.F. Packman, The Acidity of Wood, Holzforschung 14 (1960) 178–183.
[30] B.F. Tjeerdsma, M. Boonstra, a. Pizzi, P. Tekely, H. Militz, Characterisation of thermally modified wood: molecular reasons for wood performance improvement, Holz Als Roh-Und Werkstoff 56 (1998) 149–153.
[31] A. Emsley, G. Stevens, Kinetics and mechanisms of the low-temperature degradation of cellulose, Cellulose (1994) 26–56.
[32] D. Fengel, G. Wegener (Eds.), Wood: Chemistry, Ultrastructure, Reactions, De Gruyter, 1983.
[33] A. Niklasson, L.-G. Johansson, J.-E. Svensson, The influence of relative humidity and temperature on the acetic acid vapour-induced atmospheric corrosion of lead, Corros. Sci. 50 (2008) 3031–3037.
[34] J. Tètreault, J. Sirois, E. Stamatopoulou, Studies of lead corrosion in acetic acid environments, Stud. Conserv. 43 (1998) 17–32.
[35] L.T. Gibson, C.M. Watt, Acetic and formic acids emitted from wood samples and their effect on selected materials in museum environments, Corros. Sci. 52 (2010) 172–178.
[36] J.-O. Fechter, F. Englund, A. Lundin, Association between temperature, relative humidity and concentration of volatile organic compounds from wooden furniture in a model room, Wood Mat. Sci. Eng. 1 (2006) 69–75.
[37] A. van Loon, Color Changes and Chemical Reactivity in Seventeenth-century Oil Paintings, PhD Thesis, Amsterdam, The Netherlands, 2008.
[38] A. Niklasson, L.-G. Johansson, J.-E. Svensson, Atmospheric corrosion of lead, J. Electrochem. Soc. 154 (2007) C618.
[39] C.T. Chantler, K. Olsen, R.A. Dragoset, J. Chang, A.R. Kishore, S.A. Kotochigova, D.S. Zucker, X-ray Form Factor, Attenuation and Scattering Tables, Detailed Tabulation of Atomic Form Factors, Photoelectric Absorption and Scattering Cross Section, and Mass Attenuation Coefficients for $Z = 1–92$ from $E = 1–10$ eV to $E = 0.4–1.0$ MeV (2001).